IEEE Access
Multidisciplinary ⋮ Rapid Review ⋮ Open Access Journal

Received 27 October 2022, accepted 15 November 2022, date of publication 17 November 2022, date of current version 28 November 2022.

Digital Object Identifier 10.1109/ACCESS.2022.3223104

RESEARCH ARTICLE

Synthesis of Wideband Thinned Eisenstein Fractile Antenna Arrays With Adaptive Beamforming Capability and Reduced Side-Lobes

SAID E. EL-KHAMY[1], (Life Fellow, IEEE), **HUDA F. EL-SAYED**[2], AND **AHMED S. ELTRASS**[1]
[1]Electrical Engineering Department, Faculty of Engineering, Alexandria University, Alexandria 21544, Egypt
[2]Department of Basic Science, Pharos University, Alexandria 21648, Egypt

Corresponding author: Ahmed S. Eltrass (ahmed.eltrass@alexu.edu.eg)

ABSTRACT A modern design of fractal antenna arrays, called fractile array, which exhibits a fractal boundary contour within a tiled plane, is explored for enhanced array performance. In this paper, the Eisenstein fractile array is introduced to exploit the unique geometrical features of fractiles that allow multiband and wideband operation and avoid grating lobes in the radiation pattern even, in some cases, when the array elements' spacing is greater than the half wavelength. To alleviate the large number of elements and the high Side-Lobe Level (SLL) occurred at large scales, the Genetic Algorithm (GA) optimization technique is considered for thinning the proposed antenna array by estimating the optimal set of "on" and "off" elements corresponding to the minimum SLL without degrading the directivity of the radiation pattern. Also, the proposed array configuration is designed with adaptive beamforming capability using the Least Mean Square (LMS) technique. The effectiveness of the proposed GA-LMS approach is investigated by performing several MATLAB simulations under various set of array configurations. Results reveal that the suggested thinned Eisenstein fractile antenna array using GA-LMS approach is superior in terms of multiband and wideband performance, array element reduction, SLL reduction, grating lobe elimination, and beamforming capability. This elucidates the robustness of the suggested thinned Eisenstein fractile array as a promising design for multiband, wideband, compact, inexpensive, and adaptive smart antennas in modern wireless systems.

INDEX TERMS Fractal array, adaptive beamforming, Eisenstein fractile array, genetic algorithm (GA), least mean square (LMS), wideband arrays, multiband arrays.

I. INTRODUCTION

As modern wireless communication advances, designing compact antennas for a broad variety of frequency bands becomes more important [1], [2]. Antenna arrays that satisfy multiband operation and small size are desirable in various wireless applications, including cellular mobile communications, satellite systems, automotive radar systems, and other modern wireless systems [3], [4]. Designing antenna arrays that function in diverse frequency bands can be accomplished by fractal antenna arrays [5]. Fractal geometry is a concept for designing various antenna elements and developing distinct spatial function distributions for elements in antenna arrays [6]. Fractal shapes were initially employed to increase operating bandwidths and downsize antennas. Fractals possess certain features that allow them to provide a wider bandwidth; these include self-similarity and space-filling characteristics [7]. Self-similarity means that the entire shape can be divided into many subparts and each of these subparts is a replication of the whole shape in a smaller size. The effect of this feature on antennas is multiband and broadband behavior [5]. The use of fractal antenna arrays allows improving multi-beam and multiband features due to the recursive nature of fractals, which yields improved array factor properties [8].

The application of fractals in antenna arrays was investigated by developing a methodology that employs random

The associate editor coordinating the review of this manuscript and approving it for publication was Mengmeng Li.

fractals to the synthesis of quasi random arrays [9]. Like traditional antenna arrays, fractal arrays can be classified into three basic types based on their geometric patterns. They are linear, planar, and conformal fractals. Linear and planar fractal arrays are commonly developed using concentric circular ring subarray generator [10], [11]. Examples of such fractal arrays include linear Cantor, Sierpinski carpet, pentagonal, and square arrays [12], [13], [14], [15]. In [16], a technique for designing frequency-independent fractal arrays, i.e., low side-lobes and multiband, was proposed. Several studies investigated the design of Cantor fractal linear arrays [17], [18]. Planar concentric-ring Cantor arrays were developed utilizing polyadic Cantor bars which are defined by their similarity fractal dimension, number of gaps, and lacunarity parameter. Various planar fractal array configurations, with Sierpinski carpets as a basis of development, were developed [17], [18]. Sierpinski carpet and other related arrays were exploited to develop rapid algorithms that can be utilized for efficient radiation patterns, as well as adaptive beamforming [19], [20]. In these specific arrays, as the number of stages increases, so does the count of elements [19], [20]. Some modern studies investigated the synthesis of various fractal antenna array configurations that can be used in several wireless applications [5], [6]. In [21], a Multiple-Input Multiple-Output (MIMO) radar system consisting of 18 transmit and 24 receive antennas and operating in the frequency range from 77 to 81 GHz was designed based on antenna array topologies with space filling fractals, and the results revealed an enhancement in the measurement accuracy compared to traditional radar systems. In [22], a modern design of an eight-element circular fractal array was proposed for covering distinct wireless systems, such as Wi-Max (3.5–3.8 GHz), WLAN (5.15–5.85 GHz), and X-band for satellite communications (7.1–7.76 GHz).

An efficient class of deterministic arrays, called fractile arrays, which avoid grating lobes even when the array elements' spacing is just a single wavelength was introduced [23]. A fractile array is an array that exhibits a fractal boundary contour within a tiled plane. Few studies investigated plane tiling utilizing fractal shaped tiles, or fractiles, which provide all possible tile geometries that can be utilized to cover the plane, while eliminating any gaps or overlapping [24], [25]. Rare examples of fractile arrays are the Peano-Gosper, the terdragon, the 6-terdragon, the six-stage tetrahedron, and the fudge flake arrays. Compared to other conventional types of periodic planar arrays with square or rectangular cells and regular boundary contours, fractile antenna arrays provide a wider bandwidth. Note that fractile antenna arrays differ mainly from other kinds of fractal array designs explored in [1] and [22], in that the latter have regular boundaries, and their elements have a fractal pattern distribution on the inside of the array.

The difficulty in designing fractal antenna arrays stems from the fact that they require a large number of antenna elements on larger scales [26]. To alleviate the huge number of elements at large scales and as well as the large peak Side-Lobe Level (SLL), a thinning operation can be employed to switch off certain antenna elements on purpose. An added advantage to the thinning process is its ability to make the antenna array more cost effective, while providing minor trade off in beam width and directivity in comparison with fully filled arrays [27]. Several optimization algorithms were investigated for synthesizing thinned linear and planar arrays. Among which, the Particle Swarm Optimization (PSO) [28], [29], Genetic Algorithm (GA) [27], [30], [31], Simulated Annealing (SA) [32], [33], Ant Colony Optimization (ACO) [34], and Boolean Differential Evolution Algorithm (BDE) [35] were used. In [36], the binary GA technique was employed to optimize the excitations of the outer elements of planar antenna array and to reduce the number of active elements while preserving the desired radiation characteristics. In [37], a new stochastic optimization approach, called Slime Mold Algorithm (SMA), was investigated to design thinned concentric circular antenna arrays with lowest SLL and fixed HPBW. In [38], the PSO technique was investigated to minimize the number of antenna elements, element spacing, and SLL for elliptical cylindrical antenna arrays of radar systems.

Beamforming or array pattern synthesis is a major application of array processing, explored in various wireless applications, including radar, sonar, mobile communications, seismic sensing, biomedical engineering, etc. It includes designing antenna arrays with shaped beam that provide high gain in the Direction of Arrival (DOA) of a desired signal and suppress interferences in the DOA of every undesired signal to increase the signal-to-interference-plus-noise ratio (SINR) [39], [40]. Various adaptive signal processing methods, including the Least Mean Squares (LMS) and the Recursive Least Squares (RLS), were employed for array pattern synthesis of ordinary antenna arrays by calculating the optimal excitation weights for array elements that provide the desired radiation pattern [41], [42], [43], [44]. On contrast, the design of fractal arrays, in particular fractile arrays, with adaptive beamforming capability remains largely an unexplored area of research. In [45], the LMS technique was investigated for array pattern synthesis of Sierpinski carpet fractal arrays. In [46], the ACO algorithm was utilized for synthesizing thinned hexagonal and pentagonal fractal arrays, while the LMS technique was employed as an adaptive beamformer. In [47], the discrete Kalman filter was introduced as a novel adaptive beamformer for the design of linear Cantor array in wireless environment with high-jamming power.

While most of the recent ordinary antenna array designs provided reasonable radiation pattern characteristics, new fractal array configurations should be explored for multiband, wideband, and adaptive smart antennas in modern wireless systems. The aim of this research study is to introduce a new approach for the synthesis of thinned wideband fractile antenna arrays, characterized by the lowest SLL with adaptive beamforming capability. A new approach is proposed for the design of wideband and low-SLL antenna arrays using the unique geometrical characteristics of fractiles. The

GA optimization technique is considered for the design of thinned fractile arrays by finding the optimum combination of the fractile array's "on" and "off" elements, which leads to a maximum decrease in the peak SLL. To the author's knowledge, it is the first time to introduce a thinned fractile array synthesis with adaptive beamforming capability for multiband and broadband wireless applications. This paper is divided into the following sections. Section 2 introduces the design method of Eisenstein fractile antenna arrays, followed by investigating the GA optimization technique to achieve thinned and optimized fractile antenna arrays. Section 3 shows the array pattern results of the suggested thinned Eisenstein fractile arrays, followed by presenting the adaptive beamforming results of applying the GA-LMS approach to the Eisenstein fractile antenna arrays. Section 5 provides the conclusion of this research.

II. METHDOLOGY

In this study, a modern design of thinned wideband antenna arrays is introduced utilizing an efficient class of deterministic arrays, called fractile arrays, that exhibit a fractal boundary contour within a tiled plane without any gaps or overlaps [24]. The unique geometrical characteristics of fractiles can be utilized to provide better performance than their traditional periodic planar array counterparts. There are several fractal shaped tiles, or fractiles, that can be investigated to cover the plane, while eliminating any gaps or overlapping [23], [24], [48]. In this work, a new design of fractile antenna array based on the Eisenstein packing [49] is introduced, for the first time, to provide multiband operation with low SLL and without grating lobes.

The complex plane is filled with the whole set of complex numbers that include real and imaginary parts in the form of $a + ib$, where i is the imaginary. The Gaussian domain forms a square lattice, or a regular grid of points arranged orthogonally, and it represents a subset of the complex plane. The Gaussian plane is filled with the entire set of Gaussian integers, which are complex numbers in the form of $a + ib$, where both a and b are integers [49]. Unlike the Gaussian domain which forms a square lattice, the Eisenstein domain constructs a triangular lattice as shown in Fig. 1. The Eisenstein domain is filled with the entire set of Eisenstein integers, which do not line up orthogonally and take the form of $a+bw$, where both a and b are integers and $w = \frac{\left(-1+i\sqrt{3}\right)}{2}$ [49]. This means that a and b components in the Gaussian domain are shifted to $a - b/2$ and $b\sqrt{3}/2$ components in the Eisenstein domain, respectively. This represents a mapping from a square lattice of Gaussian domain to a triangular lattice of Eisenstein domain as shown in Fig. 1. The Eisenstein boundary is formed of six congruent self-similar parts, where each part contains three copies of itself, shrunk by a factor of 1/2 [24]. The fractal dimension s of the Eisenstein boundary should satisfy the condition $3(1/2)^s = 1$, yielding a fractal boundary of $s = \log 3/\log 2 > 1$. Since each Eisenstein

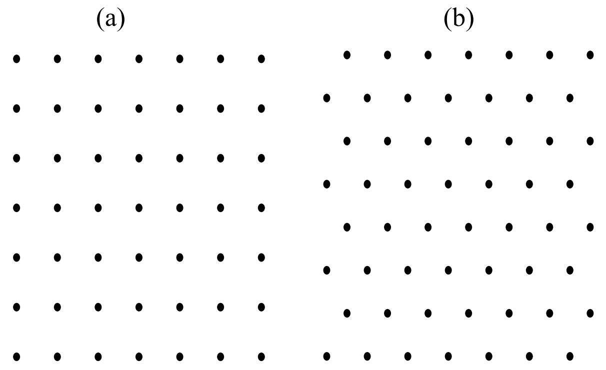

FIGURE 1. (a) Square lattice of Gaussian domain and (b) Triangular lattice of Eisenstein domain.

fraction has a corresponding Eisenstein curve that fills its interior, then the Eisenstein array belongs to the family of fractile arrays [24], [26].

The Eisenstein fractile antenna array is constructed using a ring subarray generator of three-element circular subarray generator of radius $r = \lambda/(2\sqrt{3})$ with an added element of unit current in the center of the generating subarray (see Fig. 2). Note that individual elements of the three-element circular subarray generator are located on the vertices of equilateral triangle, forming an equilateral triangular array of half-wavelength spacing on a side. This generating subarray represents a small array at growth stage $p = 1$ which is repeated many times to develop larger Eisenstein fractile arrays at higher scaling factor (i.e., $p > 1$). Fig. 2 shows the first three stages of Eisenstein fractile antenna array. Elements' locations associated with current distributions of stages 1, 2, and 3 for Eisenstein fractile array are depicted in Figs. 2a, 2b, and 2c, while their geometries are illustrated in Figs. 2d, 2e, and 2f, respectively. The minimum array spacing d_{min} between consecutive array elements is uniformly distributed along the Eisenstein curve and it remains unchanged for all stages. Fig. 3 illustrates the representation of the Eisenstein fractile array utilizing three self-similar subarray apertures.

For M concentric ring arrays with N_m elements in every single m^{th} ring, the associated far field array factor $AF(\theta, \emptyset)$ can be expressed as [8]:

$$AF(\theta, \emptyset) = \sum_{m=1}^{M} \sum_{n=1}^{N_m} I_{mn} e^{j\varphi_{mn}(\theta,\emptyset)} \tag{1}$$

where

$$\varphi(\theta, \emptyset) = kr_m sin\theta \cos(\emptyset - \emptyset_{mn}) + \alpha_{mn}$$

r_m is the radius of the m^{th} ring, θ and $\emptyset$ represent the far field point angles. $\emptyset_{mn}$, I_{mn}, and α_{mn} are the azimuthal angle, the excitation current amplitude, and excitation current phase of the n^{th} element on the m^{th} ring. $k = \frac{2\pi}{\lambda}$ is the wavenumber and λ is the wavelength.

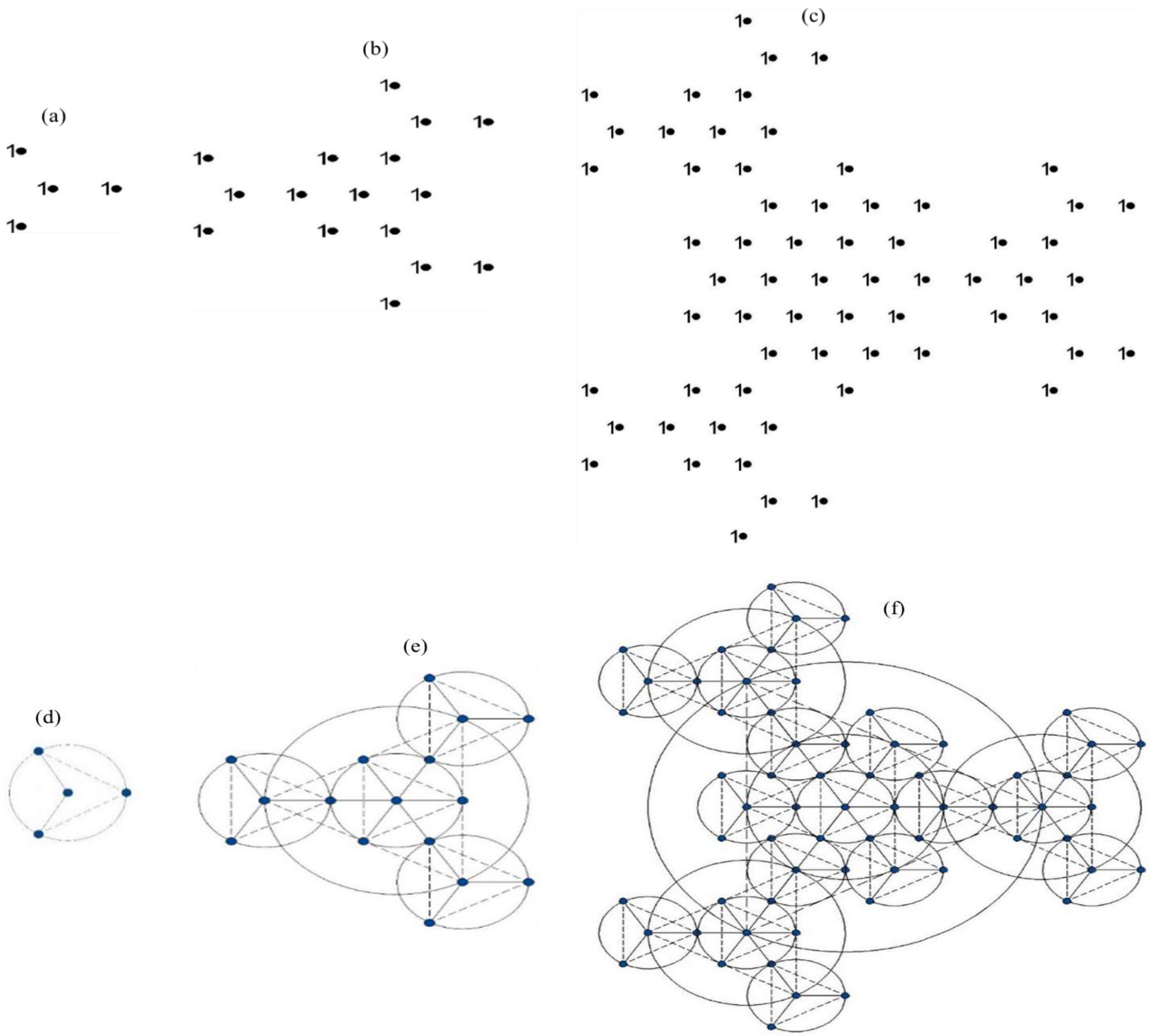

FIGURE 2. The first three stages of Eisenstein fractile antenna array. Elements' locations and geometries for stage 1 (a and d), stage 2 (b and e), and stage 3 (c and f) of Eisenstein fractile array are shown, respectively.

From equation (1), an expression for the array factor at a specific growth stage p can be deduced as follows:

$$AF_P(\theta,\emptyset)=\prod_{p=1}^{P}\left[\sum_{m=1}^{M}\sum_{n=1}^{N_m}I_{mn}e^{j\delta^{p-1}\varphi_{mn}(\theta,\emptyset)}\right] \quad (2)$$

where δ denotes the expansion factor and P represents the number of growth stages. The Eisenstein fractile antenna array is formed using a ring subarray generator of uniform three-element circular subarray generator of radius $r=\lambda/(2\sqrt{3})$ with an added element of unit current in the center of the generating subarray. Note that the subarray generator of Eisenstein fractile antenna array is rotated by an angle of $\pi/3$ from one growth stage to the next, which is not the case for standard self-scalable fractal array generator [13].

For an expansion factor δ of 2, the far field array factor of Eisenstein fractile antenna array at a specific growth stage p is given by

$$AF_P(\theta,\emptyset)=\frac{1}{4^P}\prod_{p=1}^{P}\left[1+\sum_{n=1}^{3}I_ne^{j2^{p-1}\varphi_{np}(\theta,\emptyset)}\right] \quad (3)$$

where

$$\begin{aligned}\varphi_{np}(\theta,\emptyset)&=kr_n sin\theta\cos\left(\emptyset-\emptyset_{np}\right)+\alpha_n\\&=\frac{\pi}{\sqrt{3}}sin\theta\cos\left(\emptyset-\emptyset_{np}\right)+\alpha_n,\end{aligned}$$

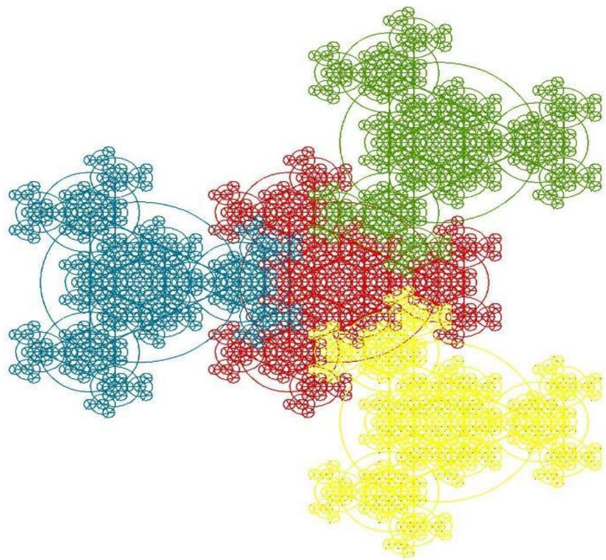

FIGURE 3. Representation of Eisenstein fractile array by three self-similar subarray apertures.

TABLE 1. The number of antenna elements, SLL, HPBW, and maximum directivity of Eisenstein fractile antenna array at growth stages $p = 2, 3, 4,$ and 5 using $d_{min} = \lambda/2, \lambda,$ and 1.5λ.

d_{min}/λ	Growth stage (p)	Number of elements	SLL (dB)	HPBW (Degree)	Directivity (dB)
0.5	2	16	-	76.73	9.39
	3	64	-25.59	36.97	15.33
	4	256	-26.29	18.29	21.10
	5	1024	-26.47	9.14	27.06
1	2	16	-22.61	37.77	13.53
	3	64	-25.59	18.69	19.63
	4	256	-26.29	9.14	25.98
	5	1024	-26.48	4.77	32.30
1.5	2	16	-22.61	25.44	13.99
	3	64	-25.60	12.32	20.62
	4	256	-26.29	6.36	27.38
	5	1024	-26.49	3.18	34.22

$$\emptyset_{np} = \frac{\pi}{3}(2n+p-3), \text{ and } \alpha_n = -\frac{\pi}{\sqrt{3}} sin\theta_0 \cos(\emptyset_0 - \emptyset_{np})$$

θ_0 and $\emptyset_0$ denote the steering angles. For Eisenstein fractile antenna array, the total count of elements N_p included in the array at certain p can be easily obtained from the relation $N_p = 4^p$.

The maximum directivity of a broadside stage p Eisenstein fractile array of isotropic sources, for the case in which $\theta_0 = 0^o$, can be expressed as [24]:

$$D_P(\theta, \emptyset) = \frac{|AF_P(\theta, \emptyset)|^2_{max}}{\frac{1}{4\pi}\int_0^{2\pi}\int_0^{\pi}|AF_P(\theta, \emptyset)|^2 \sin(\theta) d\theta d\emptyset} \quad (4)$$

III. RESULTS

The usefulness of the proposed Eisenstein fractile antenna array is investigated by carrying out MATLAB simulations under various set of array configurations and parameter regimes. Figs. 4a and 4c show the array factor patterns of Eisenstein fractile antenna array versus θ with $\emptyset = 90°$ at fixed operating frequency for different growth stages ($p = 2, 3, 4,$ and 5) using minimum element spacing $d_{min} = \lambda/2$ and λ, respectively. It can be noted that the suggested antenna array configuration has no grating lobes even when the minimum array elements' spacing is increased to λ. Note that periodicity in antenna array design leads to the formation of grating lobes at spacings of one-wavelength or greater. On contrast, the proposed Eisenstein fractile antenna array possess non-periodic element distributions with variable inter-element spacing which enables desirable radiation characteristics like avoiding grating lobes that would otherwise not be possible with traditional periodic arrays. This reveals that the unique geometrical characteristics of the proposed Eisenstein fractile antenna array, which include non-periodic arrangement of an Eisenstein fractal boundary contour within a tiled plane without any gaps or overlaps, enable avoiding grating lobes even when the array elements' spacing is increased to at least one wavelength.

Table 1 shows the number of antenna elements, the SLL, the Half-Power Beam Width (HPBW), and the maximum directivity of Eisenstein fractile antenna array at distinct growth stages $p = 2, 3, 4,$ and 5 using various minimum element spacings, including $d_{min} = \lambda/2, \lambda,$ and 1.5λ. It can be noted that for all element spacing cases, in lower growth stages (from $p = 2$ to 4), the number of elements increases significantly with increasing the growth stage (number of elements = 16, 64, and 256 for $p = 2, 3,$ and 4, respectively). This increase in the number of elements leads to a minor reduction in the SLL in the range from $p = 2$ to 4, while the SLL is nearly the same for larger growth stages ($p > 4$). Table 1 also reveals that with increasing the number of antenna elements at large scales, the HPBW is decreasing and the maximum directivity is increasing for all minimum element spacing cases of $d_{min} = \lambda/2, \lambda,$ and 1.5λ.

Figs. 4b and 4d demonstrate the array factor patterns of Eisenstein fractile antenna array at growth stage $p = 5$ for different operating frequencies using element spacing $d_{min} = \lambda/2$ and λ, respectively. One of the main advantages of fractile antenna array is that the frequency of operation can be reduced by a factor of $\delta_n$from the fixed design frequency f_o, where $n = 1, 2, \cdots, p-1$. Figs. 4b and 4d are obtained for Eisenstein fractile antenna array with $p = 5$, $\delta = 2$, and $n = 1, 2, 3,$ and 4, leading to operating frequencies $f_o, f_o/2, f_o/4,$ and $f_o/8$. Fig. 4b demonstrates that the array patterns of the proposed Eisenstein fractile array configuration preserve the same radiation pattern features at the four operating frequencies using element spacing $d_{min} = \lambda/2$. The

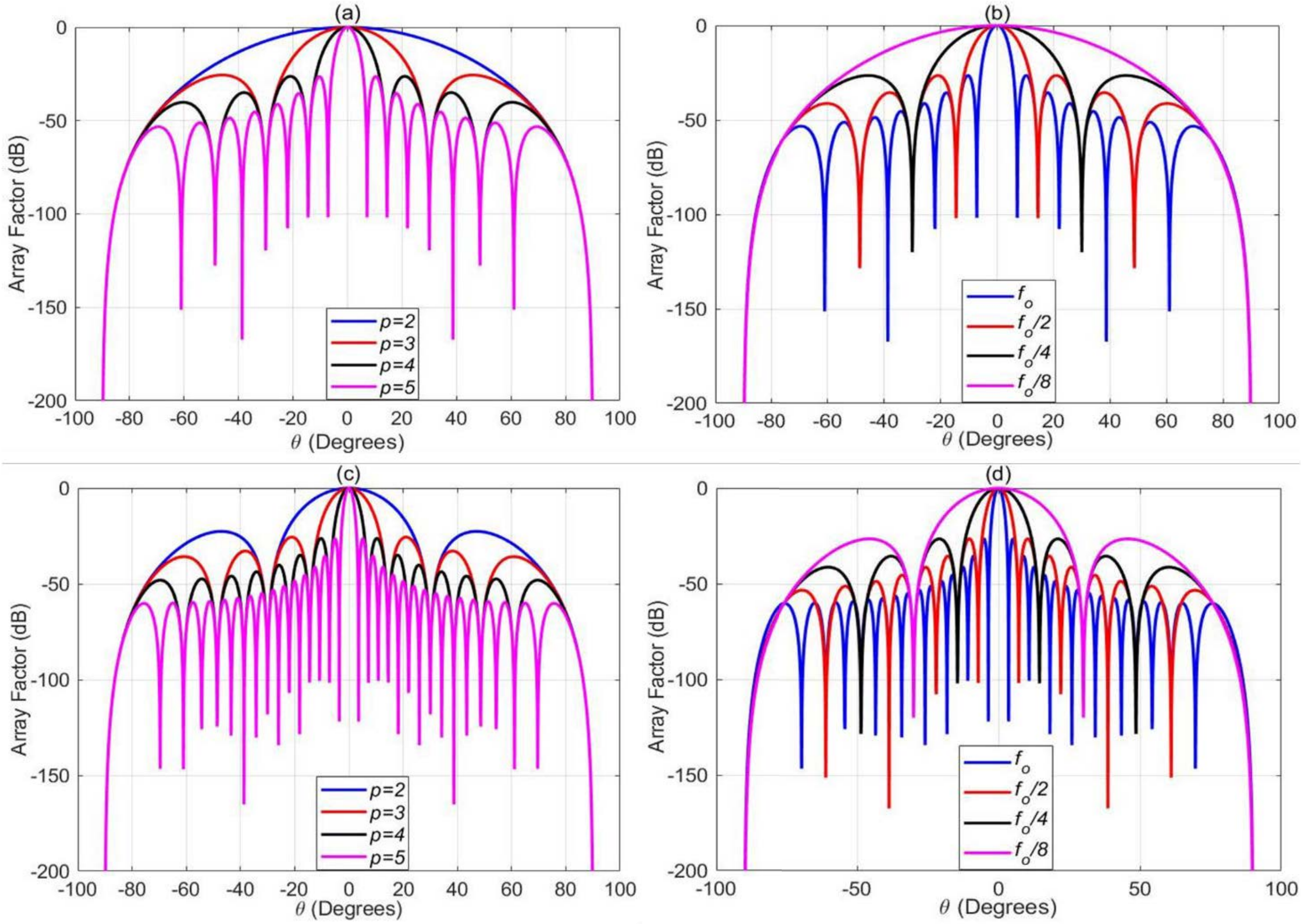

FIGURE 4. (a, c) The array factor patterns of Eisenstein fractile antenna array at fixed operating frequency for different growth stages using element spacing of $d_{min} = \lambda/2$ and λ, respectively. (b, d) The array factor patterns of Eisenstein fractile antenna array at $p = 5$ for different operating frequencies using element spacing of $d_{min} = \lambda/2$ and λ, respectively.

same efficient multiband operation is obtained using element spacing $d_{min} = \lambda$ as shown in Fig. 4d. Table 2 presents the SLL, the HPBW, and the maximum directivity of Eisenstein fractile antenna array at $p = 5$ for four distinct frequencies f_o, $f_o/2$, $f_o/4$, and $f_o/8$. As shown in Table 2, the SLL is maintained constant at multiple frequencies, while the HPBW and the maximum directivity are decreasing with the frequency increment. This reveals the efficient multiband behaviour of the proposed Eisenstein fractile antenna array design.

In order to investigate the SLL variation during scanning, the array factor pattern of the proposed Eisenstein fractile antenna array is plotted for steering angles $\theta_o = 50^o$ and 70^o as shown in Fig. 5. It can be noted that the performance of the proposed array design remains the same during the scanning operation. Table 3 summarizes the SLLs of Eisenstein fractile antenna array at different growth stages for various steering angles θ_0 using element spacing of $d_{min} = \lambda/2$. Results demonstrate that for certain growth stage, the SLL is maintained constant at multiple steering angles, which reveals the steady and efficient performance of the proposed array configuration during scanning.

TABLE 2. The SLL, HPBW, and maximum directivity of Eisenstein fractile antenna array at growth stage $p = 5$ for different operating frequencies using $d_{min} = \lambda$.

Operating frequency	$f_o/8$	$f_o/4$	$f_o/2$	f_o
SLL(dB)	- 26.47	- 26.47	- 26.47	- 26.48
HPBW (Degree)	36.97	18.29	9.14	4.77
Directivity (dB)	15.69	21.33	27.06	32.30

An important comparison is held between the proposed Eisenstein fractile antenna array and the corresponding conventional square antenna array of the same number of elements. A case study is presented, where an Eisenstein fractile antenna array at growth stage $p = 5$ with 1024 antenna elements is compared with a uniformly excited periodic 32×32 square array of the same number of antenna elements. Figs. 6a and 6b show, respectively, the array factor patterns of Eisenstein fractile antenna array at $p = 5$ and 32×32 periodic square array at distinct array element spacings, including $d_{min} = \lambda/2$, λ, and 1.5λ. Fig. 6a reveals that the proposed Eisenstein fractile antenna array design has no grating lobes for all cases under investigation, even when the minimum array elements' spacing is greater than $\lambda/2$. On contrast, Fig. 6b demostrates that for the 32×32 periodic square array, grating lobes exist when the minimum array elements' spacing exceeds $\lambda/2$. Grating lobes can be clearly observed in Fig. 6b for both cases of $d_{min} = \lambda$ and 1.5λ.

Table 4 shows the SLL and the maximum directivity of the proposed Eisenstein fractile antenna array and the 32×32 square array with the same number of elements for minimum element spacing of $d_{min} = \lambda/4$, $\lambda/2$,λ, and 1.5λ. The comparison reveals that for the same number of antenna elements, the proposed Eisenstein fractile antenna array achieves lower SLL than the corresponding conventional square antenna array for all element spacing cases ($d_{min} = \lambda/4, \lambda/2, \lambda$, and 1.5λ). It can be noted that for $d_{min} = \lambda/4$ and $\lambda/2$, the maximum directivity of conventional square array is slightly larger than the proposed Eisenstein fractile array because the conventional square array has no grating lobes at $d_{min} = \lambda/4$ and $\lambda/2$ and it concentrates the radiation pattern. Note that the space diversity of the proposed Eisenstein fractile array is comprable with the conventional square array for the same number elements (1024 antenna elements in this case as shown in Table 4). For all other cases of array elements' spacing greater than $\lambda/2$, the maximum directivity of the proposed Eisenstein fractile array is higher than its conventional square array counterpart. This reveals that for array elements' spacing greater than $\lambda/2$, the directivity of Eisenstein fractile array increases with the element spacing increase, while directivity of conventional square array drops down with the element spacing increase. This directivity drop may be caused by the appearance of grating lobes in the radiation pattern of the conventional square array. Unlike the conventional square antenna array which possess grating lobes in the radiation pattern when the array elements' spacing is greater than $\lambda/2$, the proposed Eisenstein fractile antenna array design has no grating lobes and instead it concentrates the radiation pattern and provides higher directivity than the conventional square array (see Table 4). This reveals the superior performance of the proposed fractile antenna array design over other conventional array configurations.

Fig. 7 shows the SLL variations of the proposed Eisenstein fractile antenna array with changing both the frequency of operation and the minimum array elements' spacing at growth stage $p = 5$. Results show that the SLL is nearly constant across the frequency range from f_o to $4f_o$, where f_o is the fixed design frequency. Fig. 7 demonstrates that for $f > 4f_o$ (not included in the bandwidth of interest), the SLL increases, and the grating lobes may exist. This elucidates that the suggested fractile array configuarion succeds not only to provide multiband operation at distinct frequencies scaled by δ, but also to achieve wideband operation throughout a frequency range spanning from f_o to $4f_o$. Also, Fig. 7 demonstrates that the SLL remains nearly unchanged for all cases of minimum array elements' spacing ranging between $\lambda/2$ and 2λ across

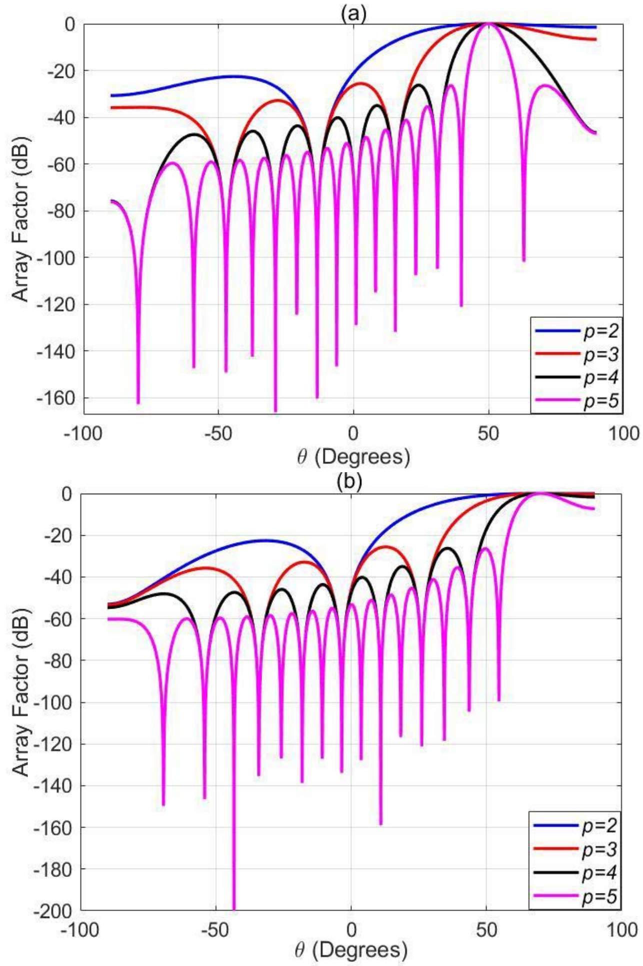

FIGURE 5. The array factor patterns of Eisenstein fractile antenna array versus θ at fixed operating frequency for different growth stages using element spacing of $d_{min} = \lambda/2$ for (a) $\theta_o = 50^o$ and (b) $\theta_o = 70^o$.

the bandwidth of interest. Moreover, it can be noted from Figs. 6 and 7 that the proposed Eisenstein fractile antenna array has no grating lobes across the entire bandwidth of interest extending from f_o to $4f_o$ for all cases of minimum array elements' spacing less than 2λ. On contrast, the conventional square array is designed at a fixed frequency and it does not possess any multiband or wideband operation. This reveals that the suggested fractile array configuration can be effectively employed to provide multiband and wideband performance, while maintaining high directivity across the bandwidth of interest.

A. THINNED FRACTILE ARRAY OPTIMIZATION RESULTS

The difficulty in implementing the proposed Eisenstein fractile antenna array comes from the relative high SLL and the huge number of antenna elements on larger scales. To alleviate such challenges, the GA optimization technique [30], [31] is investigated for thinning the Eisenstein fractile array by estimating the optimal set of "on" and "off" elements relevant to the minimum SLL without degrading the HPBW

TABLE 3. The SLL of Eisenstein fractile antenna array at different growth stages for various steering angles using element spacing of $d_{min} = \lambda/2$.

Growth stage (p)	Number of elements	SLL (dB)									
		$\theta_o = 0^o$	$\theta_o = 10^o$	$\theta_o = 20^o$	$\theta_o = 30^o$	$\theta_o = 40^o$	$\theta_o = 50^o$	$\theta_o = 60^o$	$\theta_o = 70^o$	$\theta_o = 80^o$	$\theta_o = 90^o$
2	16	-	-	-14.05	-22.61	-22.61	-22.61	-22.61	-22.61	-22.61	-22.61
3	64	-25.59	-25.59	-25.59	-25.59	-25.59	-25.59	-25.59	-25.59	-25.59	-25.59
4	256	-26.29	-26.29	-26.29	-26.29	-26.29	-26.29	-26.29	-26.29	-26.29	-26.29
5	1024	-26.47	-26.47	-26.47	-26.47	-26.47	-26.47	-26.47	-26.47	-26.47	-26.47

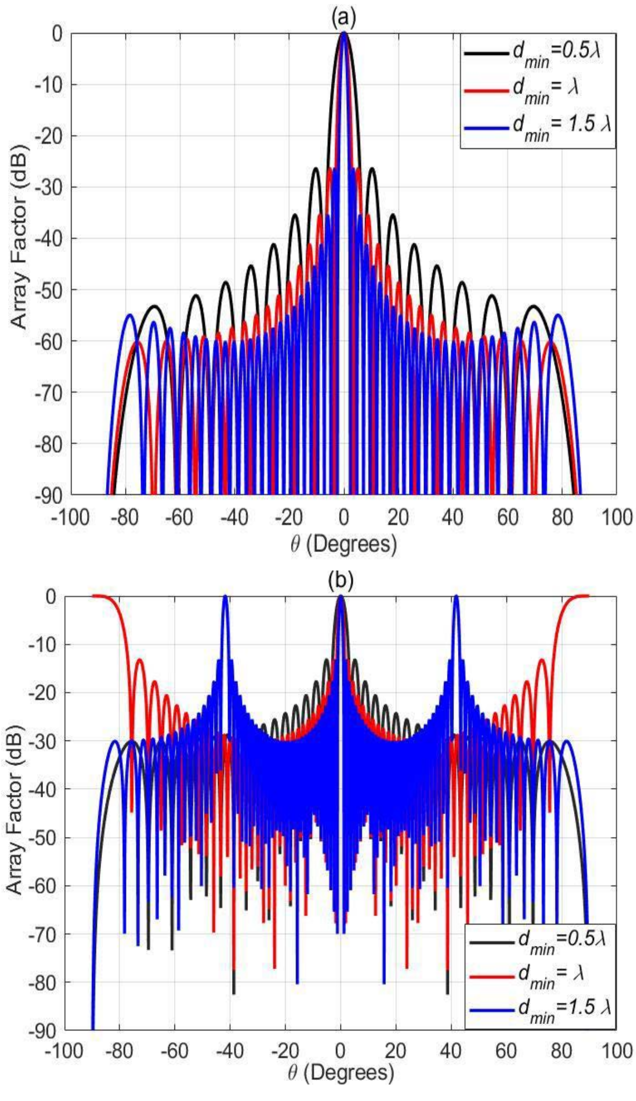

FIGURE 6. The array factor patterns of (a) Eisenstein fractile antenna array at growth stage $p = 5$, and (b) 32 × 32 periodic square array for $d_{min} = 0.5\lambda$, λ, and 1.5λ.

TABLE 4. Comparison of the SLL and the maximum directivity between the proposed Eisenstein fractile antenna array at $p = 5$ and the 32 × 32 square array for minimum array spacing of $d_{min} = \lambda/4$, $\lambda/2$, λ, and 1.5λ.

d_{min}/λ	Eisenstein fractile array at p = 5 (1024 antenna elements)		32 × 32 square array (1024 antenna elements)	
	SLL (dB)	Directivity (dB)	SLL (dB)	Directivity (dB)
0.25	- 26.46	21.33	-13.25	26.02
0.5	- 26.47	27.06	-13.3	31.98
1	- 26.48	32.30	-	24.72
1.5	- 26.49	34.22	-	28.95

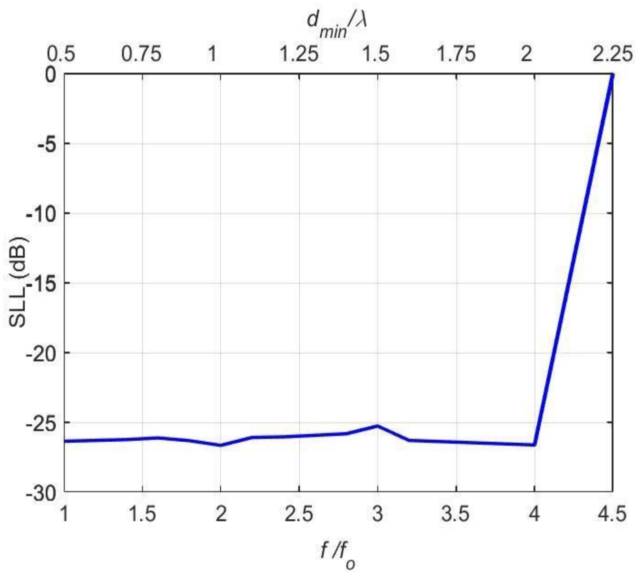

FIGURE 7. SLL variations of the proposed Eisenstein fractile antenna array with changing both the frequency of operation and the minimum array elements' spacing at growth stage $p = 5$.

and the directivity of the resulted radiation pattern. In this work, the GA is utilized to identify the optimum excitation amplitude (constrained to be 0 or 1) for every element at each growth stage to provide the minimum SLL using reduced number of elements. With GA, an initial population of individuals is generated, and the genetic mechanisms of cross-over, survival of the fittest, and mutation are utilized to acquire better and better individuals, until the best thinning configuration is achieved. The flowchart of GA optimization technique is illustrated in Fig. 8. Note that parameter setting for random optimization techniques like GA is important for

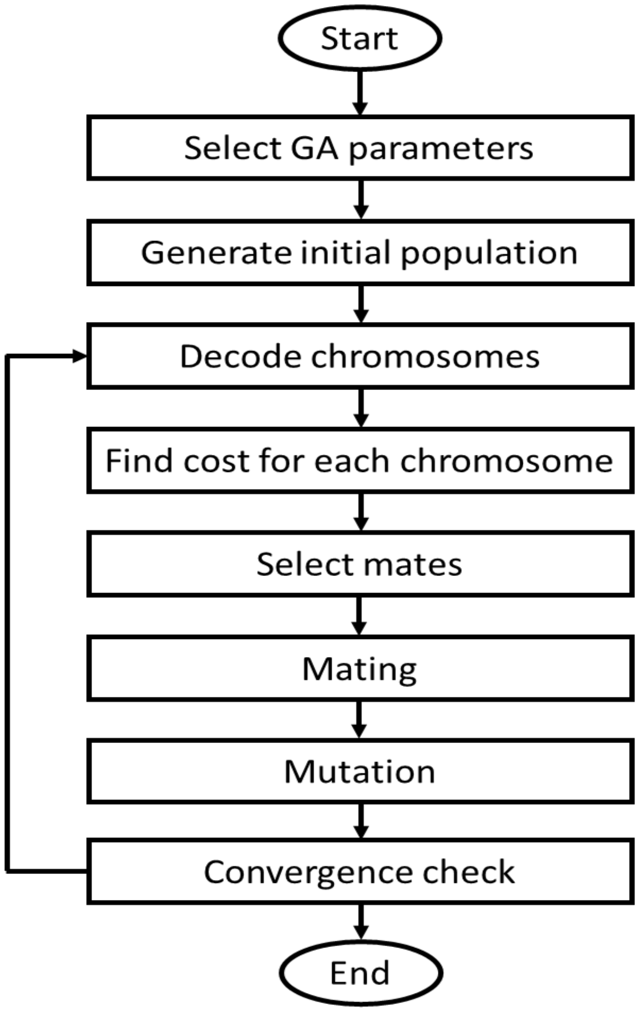

FIGURE 8. The flowchart of GA optimization technique.

obtaining acceptable convergence speed. In this work, an initial population of 30 chromosomes, maximum iterations of 100, crossover percentage of 0.5, and mutation rate of 0.01 are the optimum values for achieving the best convergence rate.

In the current study, the proposed Eisenstein fractile antenna array is thinned with GA optimization utilizing the following parameters: $d_{min} = \lambda/2$, $\delta = 2$, and$\emptyset = 90°$. Fig. 9 shows the thinned Eisenstein fractile antenna array using GA optimization at $p = 2$ and 3. It can be noted that for $p = 2$, the optimum excitation amplitudes of antenna elements that provide the lowest SLL are "0 0 1 0 1 1 0 1 1 1 0 1 0 1 1 1". This means that the thinning process with GA allows switching off 6 antenna elements out of the 16 elements at $p = 2$ and turning off 24 antenna elements out of the 40 elements at $p = 3$. This reveals the robustness of the GA optimization for acquiring the best thinning configuration relevant to minimum SLL.

Table 5 shows the number of antenna elements, SLL, HPBW, maximum directivity, and number of "off" elements of thinned Eisenstein fractile antenna array using GA optimization at $p = 2, 3, 4$, and 5 for array elements' spacing $d_{min} = \lambda/2$, λ, and 1.5λ. It can be noted that for $d_{min} = \lambda/2$, the thinning operation results in switching off around one third of the elements at all growth stages, while keeping the SLL as low as possible without remarkable degradation in the HPBW and the directivity for all array spacing cases. Note that the significant decrease in the number of antenna elements due to the thinning process leads to reduction in the weight and cost of the thinned fractile array configuration. Figs. 10a and 10b demonstrate the array factor patterns of thinned Eisenstein fractile antenna array at different growth stages and distinct operating frequencies, respectively, while fixing the array elements' spacing at $d_{min} = \lambda/2$. Fig. 10c shows the array factor patterns of the thinned Eisenstein fractile antenna array at different array elements' spacing, including $d_{min}= 0.5\lambda$, λ, and 1.5λ. Both Figs. 10b and 10c are ploted at growth stage $p = 5$. Fig. 10b elucidates that the array factor patterns of the suggested Eisenstein fractile array configuration posses similar SLL and radiation pattern features at several operating frequencies. This shows that the suggested thinned fractile array configuration succeds not only to provide the lowest SLL without degrading the HPBW and directivity using reduced number of antenna elements, but also to achieve multiband operation at different operating frequencies while avoiding any grating lobes for array elements' spacing between $\lambda/2$ and 2λ.

To elucidate the robustness of the proposed approach, the radiation pattern of the thinned Eisenstein fractile array obtained using GA is compared with that of the fully filled array version. Table 6 shows the number of antenna elements, SLL, HPBW, number of "off" elements, and maximum directivity of Eisenstein fractile antenna array with and without GA optimization at growth stages $p = 2, 3, 4$, and 5. It can be noted that the thinned array configuration with GA possesses lower number of active antenna elements than the fully filled array. Also, Table 6 demonstrates that the SLLs of the thinned Eisenstein fractile array configuration are much lower than those of the fully filled array at all growth stages. Moreover, there is a negligible degradation in the HPBW and the directivity of the thinned array configuration compared to the fully filled array at all growth stages. This reveals the outstanding performance of the suggested design in terms of reduced number of elements, SLL, weight, and cost while keeping roughly similar HPBW and directivity as the fully filled antenna array.

B. GA-LMS BEAMFORMING RESULTS

Array pattern synthesis represents an important requirement for various wireless applications. In this work, the proposed thinned Eisenstein fractile antenna array is synthsized with the adaptive beamforming capability using the LMS technique [50]. The GA was not utilized as a beamformer in the current study because it is relatively slow in reaching the steady state solution and it requires a large number of iterations. Also, some studies reported that the LMS technique achieves better directivity than GA in multipath environment,

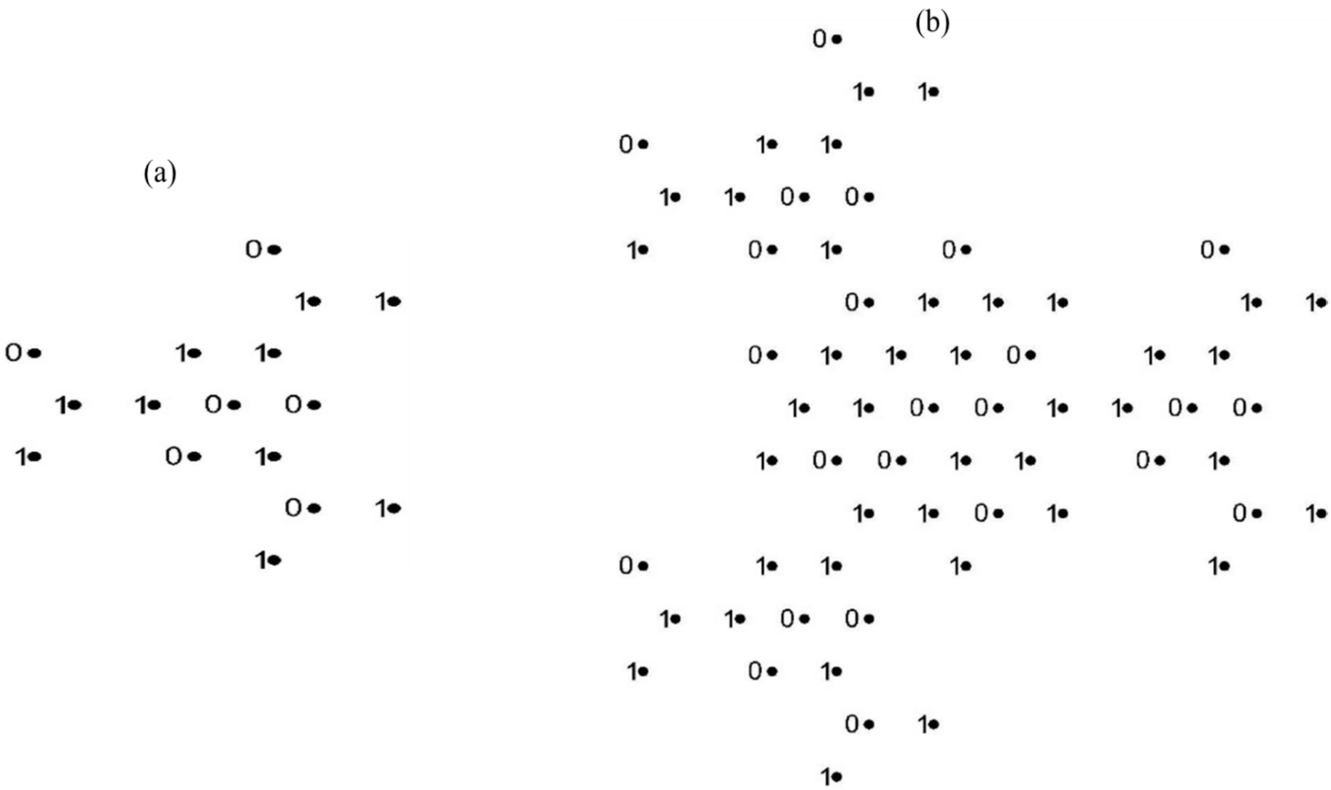

FIGURE 9. Thinned Eisenstein fractile antenna array using GA optimization at growth stages (a) $p = 2$ and (b) $p = 3$.

TABLE 5. The number of antenna elements, SLL, HPBW, maximum directivity, and number of "off" elements of thinned Eisenstein fractile antenna array using GA optimization at $p = 2$, 3, 4, and 5 for array elements' spacing of $d_{min} = \lambda/2$, λ, and 1.5λ.

d_{min}/λ	Growth stage (p)	Number of elements	SLL (dB)	HPBW (Degree)	Directivity (dB)	Number of "off" elements
0.5	2	10	-34.65	69.58	9.39	6
	3	40	-32.04	36.18	14.97	24
	4	160	-27.10	18.29	20.36	96
	5	640	-26.65	9.14	25.88	384
1	2	10	-13.98	34.59	10.48	6
	3	40	-13.98	18.29	16.33	24
	4	160	-13.98	9.14	22.38	96
	5	640	-13.98	4.77	28.17	384
1.5	2	10	-13.98	23.06	10.48	6
	3	40	-13.98	12.33	16.84	24
	4	160	-13.98	6.36	23.15	96
	5	640	-13.98	3.18	29.36	384

which provides sharper and more precise beam patterns [51]. Also, it was reported that GA is not efficient in mitigating interfering sources as LMS [51], [52]. On the other hand, the GA algorithm was proven to be an efficient for array thinning [27], [30], [31], [36] so that it was utilized for thinning the proposed array design. In the LMS approach, the weights

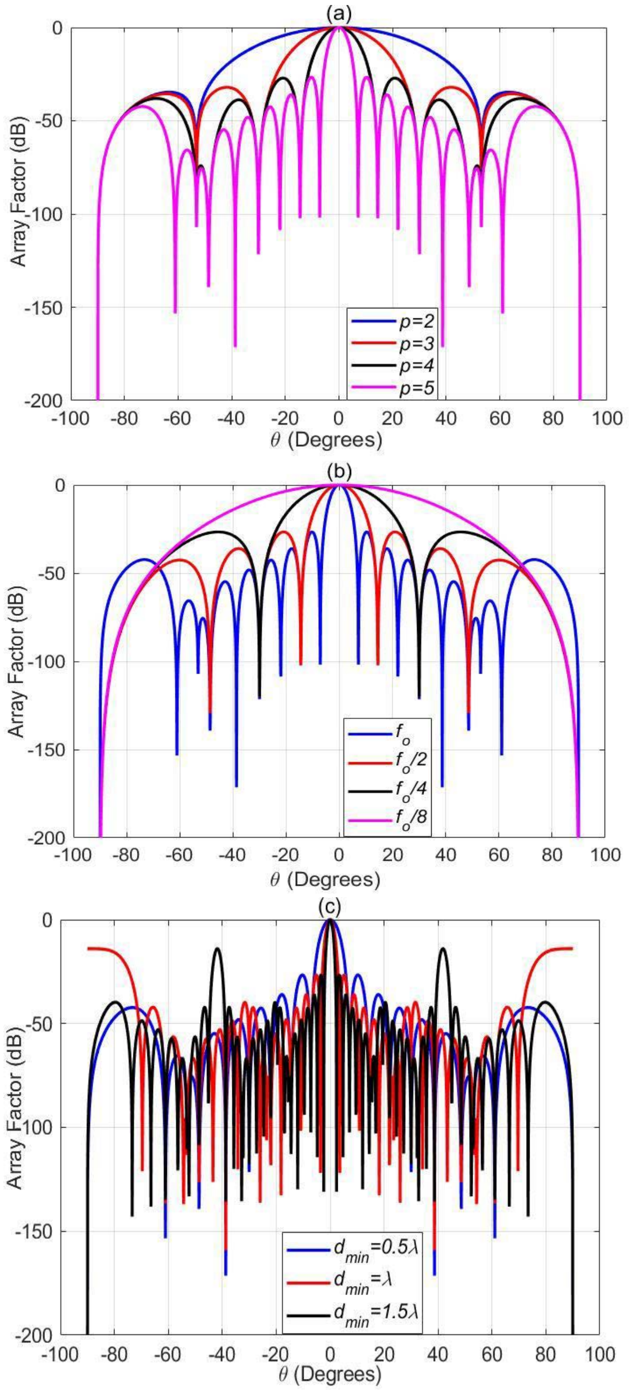

FIGURE 10. The array factor patterns of thinned Eisenstein fractile antenna array using GA optimization algorithm at fixed spacing of $d_{min} = \lambda/2$ for (a) different growth stages, and for (b) different operating frequencies. (c) The array factor patterns at array elements' spacing of $d_{min} = 0.5\lambda$, λ, and 1.5λ.

of antenna elements are calculated and updated recursively utilizing the steepest-descent method with a step size of 0.05 [53]. With LMS, the optimal excitation weights are calculated for each antenna element to obtain a shaped radiation beam that provides high gain in the DOA of a desired signal and steers the null in the DOA of every undesired signal. The impact of Additive White Gaussian Noise (AWGN) is included by performing the MATLAB simulations at specified value of SNR = 30 dB.

A combined approach of GA and LMS algorithms, called GA-LMS, is introduced to design a novel thinned Eisenstein fractile antenna array with adaptive beamforming capability and reduced SLL. Table 7 shows the optimum excitation amplitudes of thinned Eisenstein fractile antenna array using GA-LMS approach for different DOAs of desired and undesired signals at a fixed design frequency of $f_o = 1$ GHz, and SNR = 30 dB at $p = 2$. These weights are replicated for higher growth stages as illustrated in Fig. 2. Fig. 11 demonstrates the array patterns of thinned Eisenstein fractile antenna array at fixed design frequency of $f_o = 1$ GHz, and SNR = 30 dB for different growth stages using the GA-LMS approach. The DOAs of the desired and the undesired signal are (30°, 0°) for Fig. 11a and (-10°, 20°) for Fig. 11b, respectively. It can be seen from Fig. 11 that the radiation pattern features, including the main lobe peak and nulls, are nearly similar at all growth stages, which demonstrates the efficient adaptive beamforming capability of the proposed antenna array design.

Fig. 12 shows the array factor patterns of the thinned Eisenstein fractile antenna array at SNR = 30 dB for three different operating frequencies using the combined GA-LMS approach, assuming the DOAs of the desired and the undesired signal are 30° and 0°, respectively. It can be seen from Fig. 12 that the introduced GA-LMS approach provides multiband operation, in which the radiation pattern features are kept unchanged at distinct operating frequencies scaled by δ. The results reveal that the proposed thinned Eisenstein fractile antenna array configuration using GA-LMS approach is superior in terms of multiband operation, array element reduction, SLL reduction, grating lobe elimination, and beamforming accuracy. This elucidates that with the proposed GA-LMS algorithm, the designer can provide accurate dynamically shaped radiation pattern with lowest SLL and reduced number of antenna elements, while preserving the same radiation pattern features at distinct frequencies with rapid convergence rate.

C. PERFORMANCE ANALYSIS

Despite the extensive research performed in wideband and fractal antenna arrays, to the author's knowledge, it is the first time to introduce a thinned fractile array synthesis with adaptive beamforming capability for multiband and broadband wireless applications. The proposed antenna array design is compared with recent wideband antenna arrays [54], [58], and the results are summarized in Table 8. It can be noted that the proposed Eisenstein fractile antenna array achieves the lowest SLL using lower number of elements than all other wideband arrays under comparison for all minimum element spacing cases of $d_{min} = \lambda/2, \lambda$, and 1.5λ. This reveals the superior performance of the proposed Eisenstein fractile array configuration in terms of wideband performance, array element reduction, and SLL reduction. This also

TABLE 6. The number of antenna elements, SLL, HPBW, number of "off" elements, and maximum directivity of Eisenstein fractile antenna array with and without GA optimization at $p = 2, 3, 4$, and 5.

	Growth stage (p)	Number of elements	SLL (dB)	HPBW (Degree)	Directivity (dB)	Number of "off" elements
Without GA optimization	2	16	-	77.14	9.39	0
	3	64	-25.59	37.58	15.33	0
	4	256	-26.29	21.76	21.10	0
	5	1024	-26.36	9.89	27.06	0
With GA optimization	2	10	-34.65	69.58	9.39	6
	3	40	-32.04	36.18	14.97	24
	4	160	-27.10	18.29	20.36	96
	5	640	-26.65	9.14	25.88	384

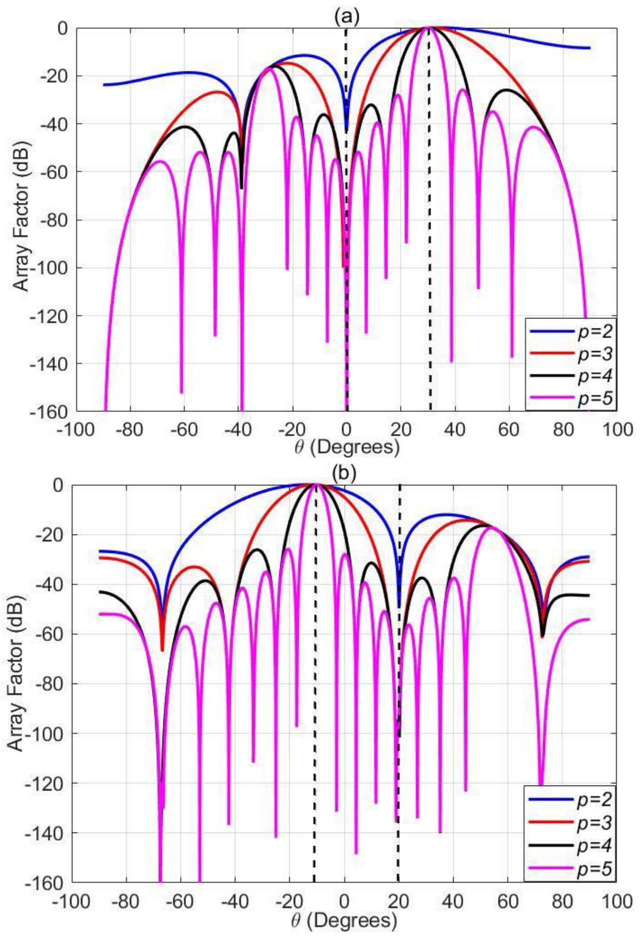

FIGURE 11. The array factor patterns of thinned Eisenstein fractile antenna array at fixed design frequency $f_o = 1$ GHz, and SNR = 30 dB for different growth stages utilizing the GA-LMS approach. The DOAs of the desired and the undesired signal are (30°, 0°) for (a) and (−10°, 20°) for (b), respectively.

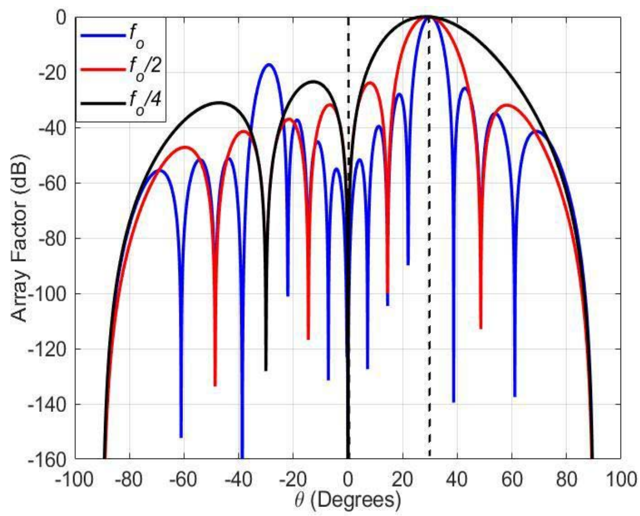

FIGURE 12. The array factor patterns of thinned Eisenstein fractile antenna array at SNR = 30 dB for three distinct frequencies utilizing the GA-LMS approach. The DOAs of the desired and the undesired signal are (30°, 0°).

TABLE 7. The optimum excitation amplitudes of thinned Eisenstein fractile antenna array using GA-LMS approach for different DOAs of desired and undesired signals at a fixed design frequency of $f_o = 1$ GHz, and SNR = 30 dB.

Optimum excitation amplitudes	DOAs of the desired and the undesired signals
W = [0, 0, 0.074, 0, 0.074, 0.117, 0, 0.114, 0.090, 0.139, 0, 0.086, 0, 0.089, 0.087, 0.136]	(30°, 0°)
W = [0, 0, 0.077, 0, 0.076, 0.116, 0, 0.114, 0.091, 0.135, 0, 0.089, 0, 0.089, 0.089, 0.134]	(-10°, 20°)

elucidates the robustness of the suggested thinned Eisenstein fractile array as a promising design for multiband, wideband, inexpensive, and dynamically shaped radiation pattern for smart antenna in modern wireless systems. Such antenna array design is desirable in various broadband wireless applications, including cellular mobile communications, satellite

TABLE 8. Comparison between the proposed Eisenstein fractile antenna array and other recent wideband antenna array designs.

Reference	Array Configuration	Number of elements	SLL (dB) $d_{min} = \lambda/2$	SLL (dB) $d_{min} = \lambda$	SLL (dB) $d_{min} = 3\lambda/2$
This work	**Wideband Eisenstein fractile antenna array**	**64**	**-25.59**	**-25.59**	**-25.60**
		256	**-26.29**	**-26.29**	**-26.29**
[54]	Wideband planar aperiodic sparse phased array	160	-14.94	-13.45	-13.45
[55]	Ultra-Wideband planar sparse phased array	270	-18.31	-----	-----
		360	-19.45	-----	_
[56]	Aperiodic concentric ring arrays for ultra-wideband	90	-24.95	-17.80	-11.40
[57]	Wideband Antenna arrays organized into randomly overlapped subarrays	201	-20.00	-----	------
[58]	Wideband fractal phased-array based on a nonuniform distribution of elements along the Peano-Gosper space-filling curve	2402	-10.96	-10.24	-7.16

systems, automotive radar systems, and other modern wireless systems.

Although the proposed fractile antenna array has been proven to be a promising design for multiband, wideband, and adaptive smart antennas in modern wireless systems, it should be examined in the future by utilizing new realistic microstrip antenna elements instead of the omnidirectional elements and simulating the proposed array configuration at certain growth stage using Ansoft HFSS software combined with MATLAB to obtain all simulated radiation patterns. Then, the experimental realization of the proposed fractile array design can be conducted and tested for various frequencies and bandwidths to compare both measurement simulation results and validate the array design. This is a goal for future investigation. Also, as the proposed array configuration works at multiple operating frequencies across large bandwidth, this study can be expanded for choosing various operating frequencies utilizing distinct switching methods. Moreover, different beamforming techniques such as GA, RLS, and Kalman filter can be examined for array pattern synthesis of the proposed Eisenstein fractile antenna array design under various SNR levels and different interference environments, and the results will be reported in the near future.

IV. CONCLUSION

In this paper, a combined approach of GA and LMS techniques, called GA-LMS, is proposed to synthesize a novel design of thinned Eisenstein fractile antenna array with adaptive beamforming capability and reduced SLL. The GA optimization technique is investigated to identify the optimum excitation amplitudes of array elements to provide the minimum SLL with reduced number of elements. To elucidate the robustness of the GA optimization approach, the radiation pattern of the thinned Eisenstein fractile array is compared with the fully filled array version in terms of the number of antenna elements, SLL, HPBW, number of "off" elements, and maximum directivity. Results reveal the superior performance of the proposed fractile array configuration over the fully filled array in terms of reduced number of elements, SLL, weight, and cost while keeping nearly similar HPBW and directivity. Moreover, the LMS adaptive beamforming method is investigated to find the optimum excitation weights that allow designing the proposed array configuration with dynamically shaped radiation patterns. Results demonstrate that with the proposed GA-LMS algorithm, the designer can provide accurate dynamically shaped radiation pattern with lowest SLL, while keeping the number of elements as low as possible. Results also show that the introduced thinned Eisenstein fractile array manages not only to provide the lowest SLL without degrading the HPBW and directivity using reduced number of antenna elements, but also to achieve both wideband and multiband operation at different frequency bands while avoiding the grating lobes for array elements' spacinggreater than $\lambda/2$. This elucidates the outstanding performance of the suggested fractile antenna array design over other conventional array configurations.

REFERENCES

[1] C. A. Balanis, *Antenna Theory Analysis and Design*, 3rd ed. Hoboken, NJ, USA: Wiley, 2005.

[2] J. Kraus and R. Marhefka, *Antennas for All Application*, 2nd ed. New York, NY, USA: McGraw-Hill, 1997.

[3] M. Khalil, A. S. Eltrass, O. Elzaafarany, B. Galal, K. Walid, A. Tarek, and O. Ahmadien, "An improved approach for multi-target detection and tracking in automotive radar systems," in *Proc. Int. Conf. Electromagn. Adv. Appl. (ICEAA)*, Sep. 2016, pp. 480–483.

[4] A. Eltrass and M. Khalil, "Automotive radar system for multiple-vehicle detection and tracking in urban environments," *IET Intell. Transp. Syst.*, vol. 12, no. 8, pp. 783–792, Oct. 2018.

[5] D. H. Werner and S. Ganguly, "An overview of fractal antenna engineering research," *IEEE Antennas Propag. Mag.*, vol. 45, no. 1, pp. 38–57, Feb. 2003.

[6] A. Karmakar, "Fractal antennas and arrays: A review and recent developments," *Int. J. Microw. Wireless Technol.*, vol. 13, no. 2, pp. 173–197, Mar. 2021.

[7] A. Praveena and V. A. S. Ponnapalli, "A review on design aspects of fractal antenna arrays," in *Proc. Int. Conf. Comput. Commun. Informat. (ICCCI)*, Jan. 2019, pp. 1–3.

[8] S. Palanisamy, B. Thangaraju, O. I. Khalaf, Y. Alotaibi, S. Alghamdi, and F. Alassery, "A novel approach of design and analysis of a hexagonal fractal antenna array (HFAA) for next-generation wireless communication," *Energies*, vol. 14, no. 19, p. 6204, Sep. 2021.

[9] Y. Kim and D. L. Jaggard, "The fractal random array," *Proc. IEEE*, vol. 74, no. 9, pp. 1278–1280, Sep. 1986.

[10] R. L. Haupt, *Antenna Arrays: A Computational Approach*. Hoboken, NJ, USA: Wiley, Sep. 2010.

[11] X. Liang, W. Zhensen, and W. Wenbing, "Synthesis of fractal patterns from concentric ring arrays," *Electron. Lett.*, vol. 32, no. 21, pp. 1940–1941, Oct. 1996.

[12] V. A. Sankar Ponnapalli and P. V. Y. Jayasree, "Design of multi-beam rhombus fractal array antenna using new geometric design methodology," *Prog. Electromagn. Res. C*, vol. 64, pp. 151–158, 2016.

[13] D. H. Werner, R. L. Haupt, and P. L. Werner, "Fractal antenna engineering: The theory and design of fractal antenna arrays," *IEEE Antennas Propag. Mag.*, vol. 41, no. 5, pp. 37–58, Oct. 1999.

[14] S. E. El-Khamy, A. S. Eltrass, and H. F. EL-Sayed, "Generator optimization for thinned fractal hexagonal and pentagonal antenna arrays using ant colony algorithm," in *Proc. 34th Nat. Radio Sci. Conf. (NRSC)*, Mar. 2017, pp. 71–78.

[15] S. E. El-Khamy, M. A. Abaul-Dahab, and M. J. Elkashlan, "A simplified Koch multiband fractal array using windowing and quantization techniques," in *IEEE Antennas Propag. Soc. Int. Symp. Transmitting Waves Prog. Next Millennium Dig. Held Conjunction With USNC/URSI Nat. Radio Sci. Meeting*, vol. 3. Salt Lake City, UT, USA, Jul. 2000, pp. 1716–1719.

[16] C. Puente-Baliarda and R. Pous, "Fractal design of multiband and low sidelobe arrays," *IEEE Trans. Antennas Propag.*, vol. 44, no. 5, pp. 730–739, May 1996.

[17] R. L. Haupt and D. H. Werner, "Fast array factor calculations for fractal arrays," in *Proc. 13th Annu. Rev. Prog. Appl. Comput. Electromagn. (ACES)*. Monterey, CA, USA: Naval Postgraduate School, Mar. 1997, pp. 291–296.

[18] D. H. Werner and R. L. Haupt, "Fractal constructions of linear and planar arrays," in *IEEE Antennas Propag. Soc. Int. Symp. Dig.*, Jul. 1997, pp. 1968–1971.

[19] D. H. Werner and P. L. Werner, "The radiation characteristics of recursively generated self-scalable and self-similar arrays," in *Proc. 16th Annu. Rev. Prog. Appl. Comput. Electromagn. (ACES)*. Monterey, CA, USA: Naval Postgraduate School, Mar. 2000, pp. 829–836.

[20] D. H. Werner and P. L. Werner, "A general class of self-scalable and self-similar arrays," in *IEEE Antennas Propag. Soc. Int. Symp. Dig. Held Conjunct With USNC/URSI Nat. Radio Sci. Meeting*, Jul. 1999, pp. 2882–2885.

[21] C. Dahl, M. Vogt, and I. Rolfes, "A MIMO radar system based on fractal antenna arrays for level measurement applications," *Adv. Radio Sci.*, vol. 19, pp. 23–29, Dec. 2021.

[22] S. S. Bhatia and J. S. Sivia, "Analysis and design of circular fractal antenna array for multiband applications," *Int. J. Inf. Technol.*, vol. 14, no. 1, pp. 243–253, Feb. 2022.

[23] D. H. Werner, W. Kuhirun, and P. L. Werner, "Fractile arrays: A new class of tiled arrays with fractal boundaries," *IEEE Trans. Antennas Propag.*, vol. 52, no. 8, pp. 2008–2018, Aug. 2004.

[24] G. A. Edgar, "Measure, topology, and fractal geometry," in *Undergraduate Texts in Mathematics*. New York, NY, USA: Springer-Verlag, 1990.

[25] B. Grfinbaum and G. C. Shephard, *Tilings and Patterns*. New York, NY, USA: W.H. Freeman and Company, 1987.

[26] M. H. Agha, M. A. Al-Adwany, O. Bayat, and H. T. Hamdoon, "Optimization of antenna array pattern for uniformly excited rectangular array via thinning," *J. King Saud Univ.-Eng. Sci.*, Feb. 2021, doi: 10.1016/j.jksues.2021.02.003.

[27] K. K. Suman, P. Ashwin, A. V. Miranda, V. S. Gangwar, and R. K. Gangwar, "An optimization technique utilizing genetic algorithm for the synthesis of large thinned planar antenna array with low peak side lobe level," in *Proc. 3rd Int. Conf. Microw. Photon. (ICMAP)*, Feb. 2018, pp. 1–2.

[28] A. Recioui, "Sidelobe level reduction in linear array pattern synthesis using particle swarm optimization," *J. Optim. Theory Appl.*, vol. 153, no. 2, pp. 497–512, May 2012.

[29] V. S. Gangwar, A. K. Singh, E. Thomas, and S. P. Singh, "Side lobe level suppression in a thinned linear antenna array using particle swarm optimization," in *Proc. Int. Conf. Appl. Theor. Comput. Commun. Technol. (iCATccT)*, Oct. 2015, pp. 787–790.

[30] J. M. Johnson and V. Rahmat-Samii, "Genetic algorithms in engineering electromagnetics," *IEEE Antennas Propag. Mag.*, vol. 39, no. 4, pp. 7–21, Aug. 1997.

[31] R. L. Haupt and D. H. Werner, *Genetic Algorithms in Electromagnetics*. Hoboken, NJ, USA: Wiley, Apr. 2007.

[32] A. Trucco, "Thinning and weighting of large planar arrays by simulated annealing," *IEEE Trans. Ultrason., Ferroelectr., Freq. Control*, vol. 46, no. 2, pp. 347–355, Mar. 1999.

[33] P. Chen, Y. Y. Zheng, and W. Zhu, "Optimized simulated annealing algorithm for thinning and weighting large planar arrays in both far-field and near-field," *IEEE J. Ocean. Eng.*, vol. 36, no. 4, pp. 658–664, Oct. 2011.

[34] O. Quevedo-Teruel and E. Rajo-Iglesias, "Ant colony optimization in thinned array synthesis with minimum sidelobe level," *IEEE Antennas Wireless Propag. Lett.*, vol. 5, pp. 349–352, 2006.

[35] L. Zhang, Y. C. Jiao, Z. B. Weng, and F. S. Zhang, "Design of planar thinned arrays using a Boolean differential evolution algorithm," *IET Microw., Antennas Propag.*, vol. 4, no. 12, pp. 2172–2178, Dec. 1999.

[36] J. R. Mohammed, "A method for thinning useless elements in the planar antenna arrays," *Prog. Electromagn. Res. Lett.*, vol. 97, pp. 105–113, 2021.

[37] A. Durmus, "The optimal synthesis of thinned concentric circular antenna arrays using slime mold algorithm," *Electromagnetics*, vol. 40, no. 8, pp. 541–553, Nov. 2020.

[38] H. S. Dawood, H. A. El-Khobby, M. M. A. Elnaby, and A. H. Hussein, "Optimized VAA based synthesis of elliptical cylindrical antenna array for SLL reduction and beam thinning using minimum number of elements," *IEEE Access*, vol. 9, pp. 50949–50960, 2021.

[39] W. Shi, Y. Li, L. Zhao, and X. Liu, "Controllable sparse antenna array for adaptive beamforming," *IEEE Access*, vol. 7, pp. 6412–6423, 2019.

[40] S. E. El-Khamy, A. M. El-Shazly, and A. S. Eltrass, "High-resolution DOA estimation using compressive sensing with deterministic sensing matrices and compact generalized coprime arrays," in *Proc. 15th Eur. Conf. Antennas Propag. (EuCAP)*, Mar. 2021, pp. 1–5.

[41] R. J. Mailloux, *Phased Array Antenna Handbook*, 2nd ed. Boston, MA, USA: Artech House, 2017.

[42] P. Saxena and A. G. Kothari, "Performance analysis of adaptive beamforming algorithms for smart antennas," *IERI Proc.*, vol. 10, pp. 131–137, Jan. 2014.

[43] S. A. Khan and S. A. Malik, "Adaptive beamforming algorithms for anti-jamming," *Int. J. Signal Process., Image Process. Pattern Recognit.*, vol. 4, no. 1, pp. 95–106, Mar. 2011.

[44] C. S. Rani, P. V. Subbaiah, K. C. Reddy, and S. S. Rani, "LMS and RLS Algorithms for smart antennas in a W-CDMA mobile communication environment," *ARPN J. Eng. Appl. Sci.*, vol. 4, no. 6, pp. 77–88, Aug. 2009.

[45] S. E. El-Khamy, A. S. Eltrass, and H. F. El-Sayed, "Adaptive beamforming synthesis for thinned fractal antenna arrays," in *Proc. 32nd Gen. Assem. Sci. Symp. Int. Union Radio Sci. (URSI GASS)*, Aug. 2017, pp. 1–4.

[46] S. E. El-Khamy, A. S. Eltrass, and H. F. El-Sayed, "Design of thinned fractal antenna arrays for adaptive beam forming and sidelobe reduction," *IET Microw., Antennas Propag.*, vol. 12, no. 3, pp. 435–441, Feb. 2018.

[47] S. E. El-Khamy, H. F. El-Sayed, and A. S. Eltrass, "A new adaptive beamforming of multiband fractal antenna array in strong-jamming environment," *Wireless Pers. Commun.*, vol. 126, pp. 285–304, May 2022, doi: 10.1007/s11277-022-09745-4.

[48] J. Ventrella, "Portraits from the family tree of plane-filling curves," in *Proc. Bridges, Math., Art, Music, Archit., Educ., Culture*. Linz, Austria: Tessellations Publishing, Jul. 2019, pp. 123–130. [Online]. Available: http://archive.bridgesmathart.org/2019/bridges2019-123.html

[49] G. Helmberg, "On the Eisenstein packing of the complex plane," *Math. Intelligencer*, vol. 37, no. 2, pp. 27–33, Jun. 2015.

[50] A. H. Sayed, *Fundamentals of Adaptive Filtering*. New York, NY, USA: Wiley, 2003.

[51] A. I. Mohsin, A. S. Daghal, and A. H. Sallomi, "A beamforming comparative study of least mean square, genetic algorithm and grey wolf optimization algorithms for multipath smart antenna system," *TELKOMNIKA (Telecommun. Comput. Electron. Control)*, vol. 18, no. 6, pp. 2911–2920, 2020.

[52] D. Burgos, R. Lemos, J. Kunzler, and H. Silva, "Adaptive beamforming for moving targets using genetic algorithms and a CDMA reference signal," in *Proc. IEEE Colombian Conf. Commun. Comput. (IEEE COLCOM)*, May 2015, pp. 1–5.
[53] F. B. Gross, *Smart Antennas for Wireless Communications With MATLAB*. New York, NY, USA: McGraw-Hill, 2005.
[54] S. Hu, C. Shu, X. Chen, and K. Wang, "Element mutual coupling effect in a wideband planar aperiodic sparse phased array," in *Proc. 14th Eur. Conf. Antennas Propag. (EuCAP)*, Mar. 2020, pp. 1–3.
[55] P. X. Li and P. F. Gu, "Fast sparse synthesis of large-scale arrays in wideband and wide angle scanning," in *Proc. Int. Conf. Microw. Millim. Wave Technol. (ICMMT)*, Sep. 2020, pp. 1–3.
[56] M. A. Panduro, A. Reyna, and D. H. Covarrubias, "Non-uniform concentric rings design for ultra-wideband arrays," *Sensors*, vol. 19, no. 10, p. 2262, May 2019.
[57] D. Bianchi, S. Genovesi, and A. Monorchio, "Randomly overlapped subarrays for angular-limited scan arrays," *Prog. Electromagn. Res. C*, vol. 68, pp. 129–139, 2016.
[58] T. G. Spence, D. H. Werner, and J. N. Carvajal, "Modular broadband phased-arrays based on a nonuniform distribution of elements along the Peano–Gosper space-filling curve," *IEEE Trans. Antennas Propag.*, vol. 58, no. 2, pp. 600–604, Feb. 2010.

SAID E. EL-KHAMY (Life Fellow, IEEE) received the B.Sc. (Hons.) and M.Sc. degrees from Alexandria University, Alexandria, Egypt, in 1965 and 1967, respectively, and the Ph.D. degree from the University of Massachusetts, Amherst, MA, USA, in 1971. He has been the Teaching Staff of the Department of Electrical Engineering, Faculty of Engineering, Alexandria University, since 1972, and was appointed as a full-time Professor, in 1982, and as the Chairperson of the Electrical Engineering Department, from September 2000 to September 2003, where he is currently an Emeritus Professor. He took part in the organization of many local and international conferences, including the yearly series of NRSC (URSI) conference series (1990–2019), ISCC 1995, ISCC 1997, ISSPIT 2000, MELECON 2002, and IEEE GCIoT 2019. He took part in many IEEE Region 8 activities as well as URSI general assemblies. He has published about 400 scientific papers in national and international conferences and journals. His current research interests include wireless multimedia communications, wave propagation, smart antenna arrays, modern signal processing techniques, image processing, and security watermarking techniques. He has earned many national and international research awards among which are the R. W. P. King Best Paper Award of the Antennas and Propagation Society of IEEE, in 1980; the Egypt's State Engineering Encouraging Research Award for two times, in 1980 and 1989, respectively; the Abdel-Hamid Schoman–Kingdom of Jordan Award for Engineering Research, in 1982; the State Scientific Excellence Award in Engineering Sciences, in 2002; the Alexandria University Appreciation Award of Engineering Sciences, in 2003; the State Appreciation Award of Engineering Sciences, in 2004; as well as the IEEE Region 8 Volunteer Award, in 2010. In 2016, he was honored by the Egypt's National Radio Science Committee of URSI and was selected as the Radio Science recognized figure of the year. Also, in 2016, he was announced to be the "The Distinct Scientist of Alexandria University, in Engineering Sciences."

HUDA F. EL-SAYED received the B.Sc. and M.Sc. degrees from Alexandria University, Alexandria, Egypt, in 2006 and 2017, respectively. She is currently pursuing the Ph.D. degree in electrical engineering with the Faculty of Engineering, Alexandria University. She is also a Teaching Assistant with the Electronics and Communication Department, Pharos University, Alexandria. Her research interests include wave propagation, smart antenna arrays, and modern signal processing techniques.

AHMED S. ELTRASS received the B.Sc. and M.Sc. degrees in electrical engineering–communication and electronics from the Faculty of Engineering, Alexandria University, in 2006 and 2010, respectively, and the Ph.D. degree in electrical engineering from Virginia Tech University, USA, in 2015. From 2006 to 2011, he was a Teaching and Research Assistant with the Electrical Engineering Department, Alexandria University. He was also a Research and Teaching Assistant with Virginia Tech University, during his Ph.D. study (2011–2015). He designed and performed several remote sensing experiments using several radars over all the world, such as the Arecibo Observatory and the MIT Haystack Observatory. He had a collaboration with STAR Laboratory, Stanford University, to model the Cassini spacecraft backscattered data of the surface of Titan (largest moon of Saturn) and to investigate its surface slope and dielectric constant. He had also a collaboration with MIT and SuperDARN Virginia Tech scientists to develop a mastery of utilizing GNSS signals, the Global Positioning System (GPS) in particular, to access space weather processes from phase delay and scintillations measurements. Also, he was instrumental in setting up the Virginia Tech GNSS Laboratory, now a multi-million-dollar facility, from 2013 to 2015. He has been the Teaching Staff of the Department of Electrical Engineering, Faculty of Engineering, Alexandria University, as an Assistant Professor, since 2015, and he was promoted to an Associate Professor, in 2020. He took part in many local and international organization of including URSI Senior, NRSC, and IEEE membership. His research interests include signal processing in communication systems, adaptive antenna arrays, and biomedical signal processing.